

Temporal full-colour tuning through non-steady-state upconversion

Renren Deng¹, Fei Qin², Runfeng Chen³, Wei Huang^{3,4*}, Minghui Hong^{2*} and Xiaogang Liu^{1,5*}

Developing light-harvesting materials with tunable emission colours has always been at the forefront of colour display technologies^{1–3}. The variation in materials composition, phase and structure can provide a useful tool for producing a wide range of emission colours, but controlling the colour gamut in a material with a fixed composition remains a daunting challenge^{4,5}. Here, we demonstrate a convenient, versatile approach to dynamically fine-tuning emission in the full colour range from a new class of core-shell upconversion nanocrystals by adjusting the pulse width of infrared laser beams. Our mechanistic investigations suggest that the unprecedented colour tunability from these nanocrystals is governed by a non-steady-state upconversion process. These findings provide keen insights into controlling energy transfer in out-of-equilibrium optical processes, while offering the possibility for the construction of true three-dimensional, full-colour display systems with high spatial resolution and locally addressable colour gamut.

The ultimate challenge in encoding, manipulating and controlling colour in materials science is to develop a universal responsive material capable of emitting a broad spectrum of colours that can be accessed remotely on demand using external stimuli such as light, pressure, magnetic and electric fields. The development of multicolour-emitting materials may lead to many revolutionary applications in a wide array of research fields, including complex data analysis, information storage, biological sensing, as well as graphics imaging and display. For instance, the realization of such optical materials in display technology allows for a display with a much higher resolution than conventional display equivalents that rely on blending pixels of three primary colours, red–green–blue (RGB), for pixilated colour display. Notably, for two-dimensional pixilated RGB or volumetric three-dimensional full-colour displays, the blending of individual RGB elements as one colour pixel is often constrained by the requirement for devices with a specific pixel configuration and manufacture^{4,5}.

Conventional approaches utilizing specially designed organic dyes or semiconducting quantum dots may be implemented where the emission colour is modulated by tuning excitation wavelengths or controlling the power density of the excitation^{6,7}. These methods, however, suffer from limitations associated with the need for multiple excitation sources or the difficulty in providing variable emission colours with consistent brightness. Despite enormous research efforts, there has yet to emerge a viable solution feasible for dynamic multicolour modulation in a single material over the entire range of possible chromaticities.

The significant development of lanthanide-doped nanomaterials over the past few years has led to the implementation of new platforms where multicolour tuning tasks can be addressed^{8–14}. Intriguingly, a single lanthanide activator featuring ladder-like-arranged energy levels can produce a set of emission bands that span the wavelength range from ultraviolet to near-infrared (NIR)^{15–21}. An appealing feature of these nanomaterials is that the emission colour can be controlled under single wavelength excitation by tailoring the intensity ratio of different emission peaks²¹. However, this colour tuning technique would require stringent experimentation involving repeated trials to obtain optimal dopant concentrations²². Here, we demonstrate a pulse-width-modulated approach that offers exquisite control over the emission colour of lanthanide-doped upconversion nanocrystals. Our approach is based on the dynamic control of energy transfer via a non-steady-state upconversion process by using a new class of pulse-width-sensitive nanocrystals with specially designed multilayer core-shell structures.

In our design, hexagonal-phase NaYF₄ was chosen as the host material for the synthesis of colour-tunable core-shell nanocrystals (Fig. 1a). We developed a layer-by-layer procedure and incorporated five sets of lanthanide ions (Yb³⁺, Nd³⁺, Tm³⁺, Ho³⁺ and Ce³⁺) into specific layers at precisely defined concentrations (Supplementary Materials and Methods). Notably, Yb³⁺ and Nd³⁺ were used as efficient sensitizers for harvesting NIR light excitation at 980 and 808 nm, respectively. Tm³⁺ was confined in the inner shell layer of the nanocrystals to make the blue emission possible, while doping with Ho³⁺ in the outer shell layer ensured the generation of red or green emissions. Note that Ce³⁺ was co-doped with Ho³⁺ in the same shell layer to facilitate the red emission of Ho³⁺ by modifying its energy depletion pathway. The blue- and red/green-emitting layers were separated by an interlayer of NaYF₄ to prevent the cross-relaxation of excitation energy between Tm³⁺ and Ho³⁺. To minimize energy loss induced by surface quenching, we introduced the NaYF₄ coating at the outermost layer of the nanocrystals (Supplementary Scheme 1). Transmission electron microscopy (TEM) showed the as-synthesized nanocrystals to have a short rod shape (Fig. 1a). The nanocrystals were 44 nm long and 30 nm wide, on average (Supplementary Fig. 1). The hexagonal phase of the as-synthesized nanocrystals was confirmed by X-ray powder diffraction (Supplementary Fig. 2).

We next measured the luminescent properties of the multilayer nanocrystals. On 808 nm excitation with a continuous-wave (c.w.) diode laser, the nanocrystals gave rise to a dominant blue emission band at 470 nm, which can be attributed to the ¹G₄ → ³H₆ transition of Tm³⁺. However, intriguingly, when irradiated at 980 nm with a

¹Department of Chemistry, National University of Singapore, Singapore 117543. ²Department of Electrical and Computer Engineering, National University of Singapore, Singapore 117583. ³Key Laboratory for Organic Electronics and Information Displays & Institute of Advanced Materials, Jiangsu National Synergistic Innovation Center for Advanced Materials, Nanjing University of Posts & Telecommunications, Nanjing 210023, China. ⁴Key Laboratory of Flexible Electronics & Institute of Advanced Materials, Jiangsu National Synergistic Innovation Center for Advanced Materials, Nanjing Tech University, Nanjing 211816, China. ⁵Institute of Materials Research and Engineering, Agency for Science, Technology and Research, Singapore 117602.

*e-mail: iamwhuang@njtech.edu.cn; elehmh@nus.edu.sg; chmlx@nus.edu.sg

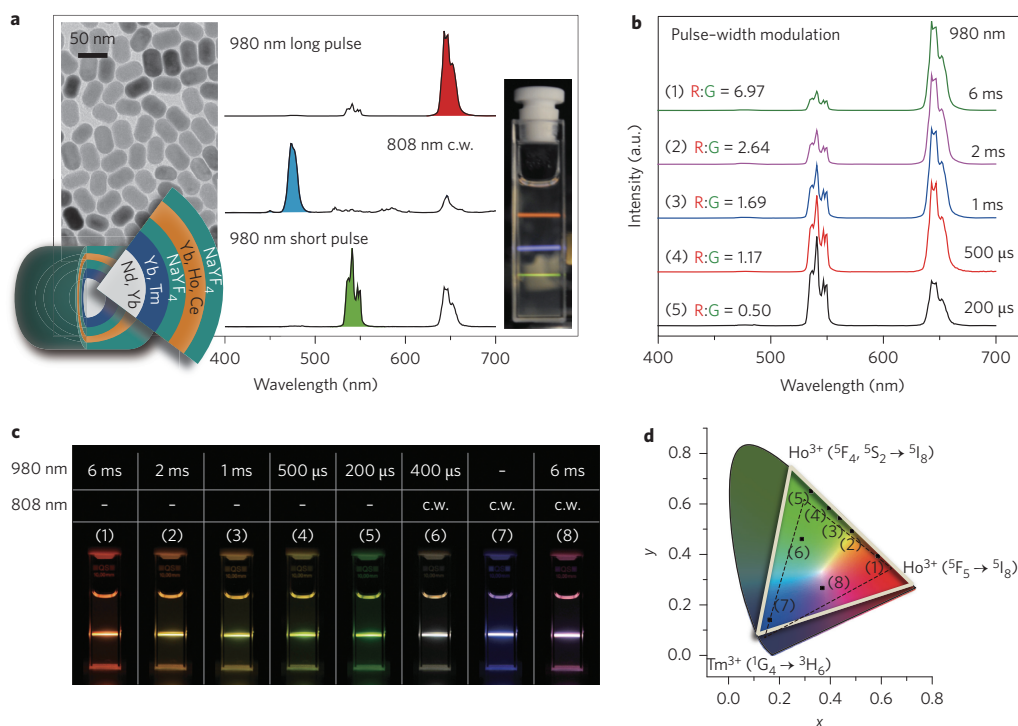


Figure 1 | Temporal multicolour tuning in NaYF₄-based core-shell nanocrystals. **a**, Design of NaYF₄-based core-shell nanocrystals capable of emitting tunable colours when irradiated with NIR lasers. Left inset: Representative TEM image of the as-synthesized nanocrystals and schematic drawing showing the layout of multilayer structures. Main panel: Upconversion emission spectra of the colloidal nanocrystals under excitation with a 980 nm pulsed laser (100 Hz, 6 ms or 100 Hz, 200 μ s) and an 808 nm c.w. laser. Right inset: Corresponding photograph showing visible RGB colour emissions by the same nanocrystals dispersed in cyclohexane upon NIR excitation. **b**, Upconversion emission spectra of the nanocrystals obtained through the use of different pulse durations, demonstrating the temporal tuning of red and green emission intensities. **c**, Luminescence photographs showing multicolour tuning (1–8) of the sample through combined use of 980 and 808 nm lasers. **d**, Corresponding colour gamut of the emission colours (marked by the outer triangle) from the sample shown in **c**, compared to the colour spaces (marked by the inner triangle) accessible by conventional high-definition televisions.

diode laser, these nanocrystals showed marked suppression in the blue emission, while exhibiting a weak green emission band at 541 nm and a strong red emission band at 646 nm. The green and red emission bands observed can be ascribed to the ³F₄, ⁵S₂ → ⁵I₈ and ⁵F₅ → ⁵I₈ transitions of Ho³⁺, respectively. Remarkably, the green/red emission intensity ratio can be tuned by using a pulsed diode laser with different pulse widths. For instance, a relatively long pulse (6 ms, 100 Hz) yielded a red/green ratio of 7, providing a visible red emission from the colloidal nanocrystals. In contrast, on decreasing the pulse width (200 μ s, 100 Hz), an intense green emission was provided as a result of a markedly reduced red/green intensity ratio (~0.5) (Fig. 1a,b). By adjusting the pulse width within the range of 200 μ s to 6 ms, we could therefore achieve dynamic control of the emission colour from green to red via control of this red/green ratio (Fig. 1b, Supplementary Fig. 3). Moreover, when combined with 808 nm c.w. laser excitation, the dual-laser system enabled us to extend the colour gamut beyond the three primaries (Fig. 1c, Supplementary Fig. 4). Because of the narrow emission bandwidths of Ho³⁺ and Tm³⁺, highly saturated RGB colours can be generated, allowing access to colour spaces much wider than achievable by conventional high-definition televisions (Fig. 1d, Supplementary Table 1)²³. Note that the doping of Nd³⁺, Tm³⁺ and Ho³⁺/Ce³⁺ in dissimilar layers is critical for obtaining multi-primary emission colours. Control experiments on nanocrystals without the core-shell structure revealed complete quenching of Tm³⁺ emission, confirming that the core-shell structure prevents cross-relaxation between Tm³⁺ and Ho³⁺ (Supplementary Fig. 5).

Figure 2 presents the proposed upconversion mechanisms that give rise to fine colour-tunability of the as-synthesized multilayer nanocrystals. The blue emission observed is clearly ascribed to an Nd³⁺-sensitized upconversion process, in which the excitation energy absorbed by Nd³⁺ on excitation at 808 nm is transferred to Tm³⁺ via Yb³⁺-mediated energy migration. As a result, activator emission at 470 nm through a three-photon upconversion process can be generated from the ¹G₄ state of Tm³⁺ (Fig. 2, Supplementary Fig. 6)^{24,25}. An open question remains on how the colour-tunable emission from Ho³⁺ is achieved with 980 nm excitation with different pulse widths.

The key mechanism responsible for colour-tunable Ho³⁺ emission can be interpreted in terms of a non-steady-state upconversion process, in which deactivation of the excitation energy and the energy transfer process occur at different rates. As the population of excited states at a particular energy level requires sequential pumping of its lower-lying energy levels²⁶, activator emission from distinct energy levels may take place at different time intervals. It is important to note that, because of the complex radiative and non-radiative transitions of the 4f electrons in excited lanthanide ions, it may take several milliseconds for the population of different energy levels to reach their steady states²⁷.

For illustration, let us consider the case of Ho³⁺, an activator that requires prior population of its ⁵I₇ state in order to subsequently pump its ⁵F₅ state for red emission (Fig. 2). However, the energy state of ⁵I₇ cannot be directly pumped through a two-step energy transfer from Yb³⁺ to Ho³⁺. Instead, an extra step of energy transfer,

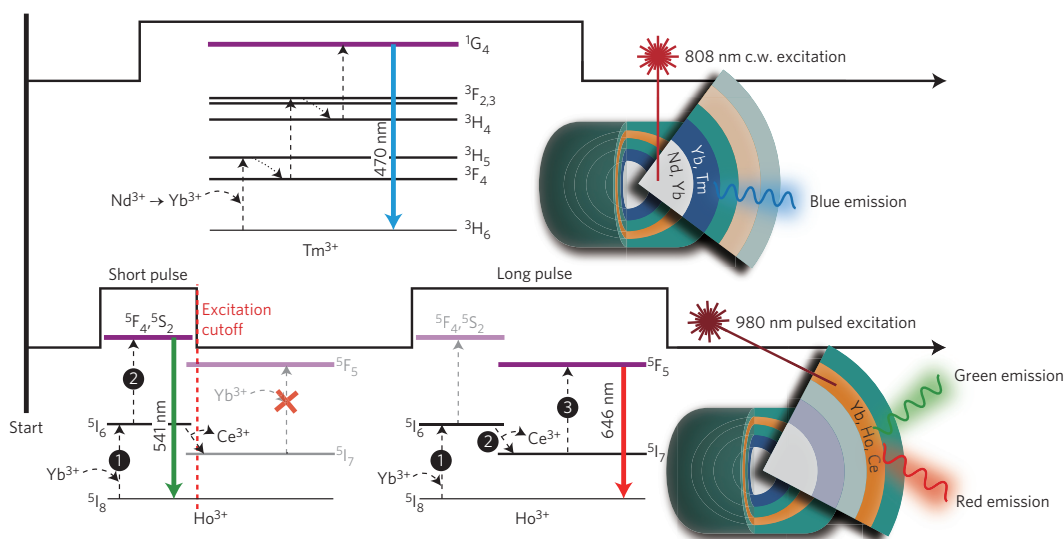


Figure 2 | Schematic representation detailing the non-steady-state upconversion mechanisms. Proposed upconversion mechanisms for blue emission generated from a $\text{Nd}^{3+}\text{-Yb}^{3+}\text{-Tm}^{3+}$ triply-doped system under 808 nm c.w. laser excitation (top) and green/red emissions from a $\text{Yb}^{3+}\text{-Ho}^{3+}\text{-Ce}^{3+}$ triply-doped system under 980 nm pulsed laser excitation (bottom). When exposed to the 808 nm c.w. laser, Nd^{3+} dopants first absorb the excitation energy and then transfer it to Yb^{3+} . Subsequently, the $^1\text{G}_4$ state of Tm^{3+} is populated by sequential energy transfer from the excited Yb^{3+} ions, resulting in blue emission at 470 nm. In the case of 980 nm pulsed laser excitation, Yb^{3+} ions serve as sensitizers to absorb 980 nm photons, followed by non-radiative energy transfer and activator emission from Ho^{3+} . The green emission at 541 nm is achieved by populating the $^5\text{F}_4, ^5\text{S}_2$ states of Ho^{3+} through a two-step energy transfer process ($\text{Yb}^{3+} \rightarrow \text{Ho}^{3+}$). It should be noted that under short-pulsed excitation the red emission at 646 nm from Ho^{3+} cannot be directly activated by Yb^{3+} , which is attributed to the delayed deactivation of the excitation energy from the $^5\text{I}_6$ state of Ho^{3+} to its lower $^5\text{I}_7$ state. By comparison, long-pulsed excitation promotes the population of the $^5\text{F}_5$ state of Ho^{3+} through a three-step energy transfer process by continued pumping of the excited Ho^{3+} ion from its $^5\text{I}_7$ state. Notably, the population of the excitation energy at the $^5\text{I}_7$ state is facilitated by a Ce^{3+} -mediated cross-relaxation process.

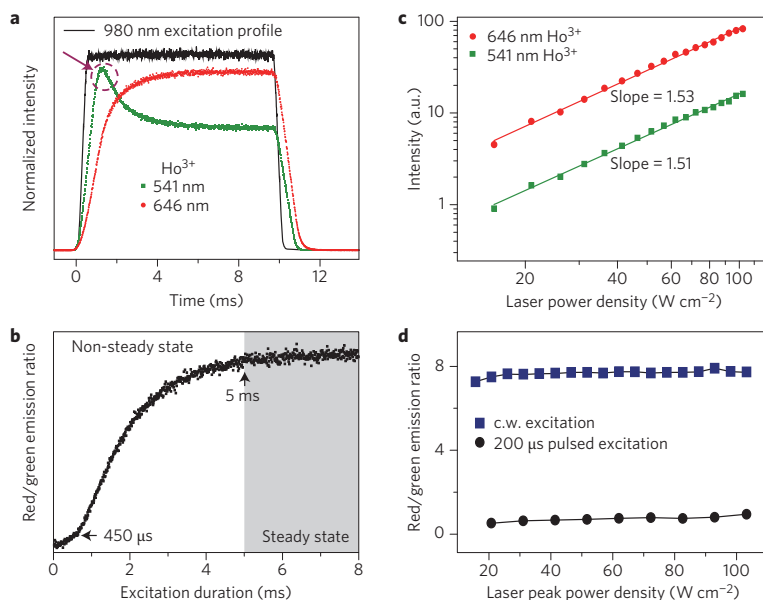


Figure 3 | Time-dependent and power-dependent measurement of colour-tunable core-shell nanocrystals. **a**, Time-dependent Ho^{3+} emission profiles of the as-synthesized core-shell nanocrystals at 541 and 646 nm upon pulsed excitation at 980 nm with a duration of 10 ms. Note that the abrupt intensity drop (marked by a dashed circle) of the 541 nm emission after 1 ms of excitation suggests an exceedingly fast depletion of the excitation energy in the $^5\text{F}_4, ^5\text{S}_2$ energy states of Ho^{3+} . The highest intensities of the 541 and 646 nm emissions have been normalized to the same level for better comparison. **b**, Corresponding red/green emission intensity ratio measured as a function of excitation duration, indicating that upconversion multicolour fine-tuning can be achieved by adjusting the excitation duration within the non-steady state (<5 ms). **c**, Power density dependence of the upconverted Ho^{3+} emission at 541 and 646 nm, showing a two-photon upconversion process for both red and green emissions. **d**, Power density dependence of the red/green emission intensity ratio obtained upon excitation of the core-shell nanocrystals at 980 nm with a c.w. laser and a pulsed (200 μs) laser.

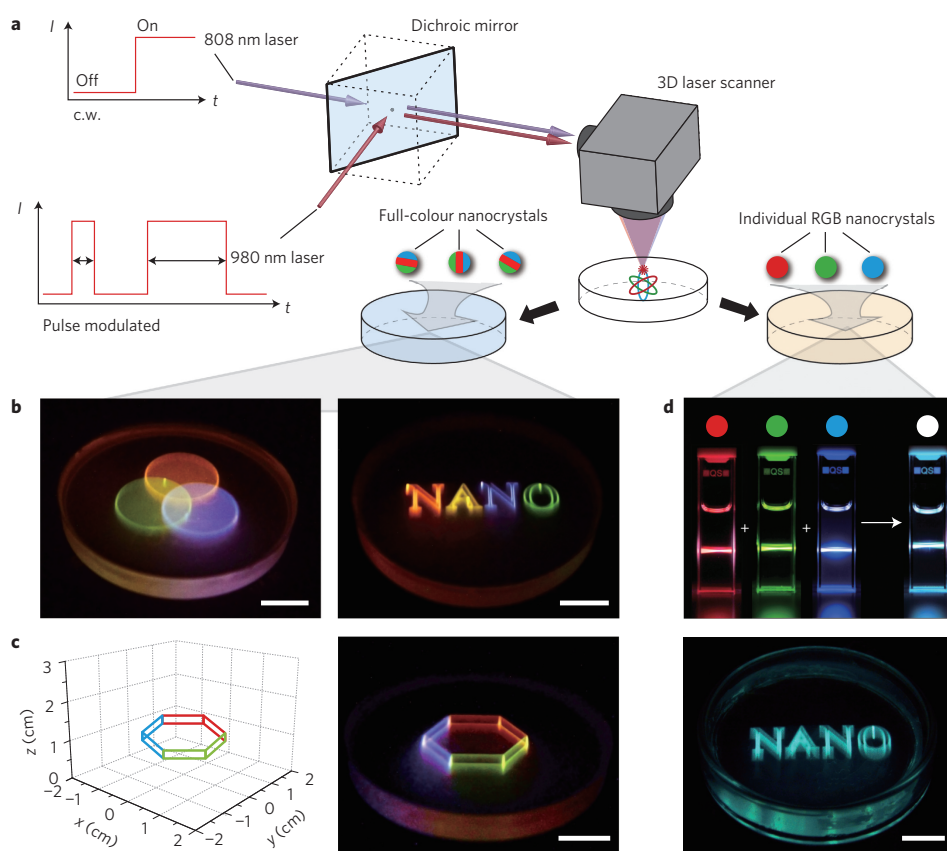


Figure 4 | Demonstration of full-colour volumetric three-dimensional display in nanocrystal/PDMS composite materials. **a**, Schematic of the experimental set-up for volumetric three-dimensional full-colour display. Briefly, a 980 nm pulsed laser and an 808 nm c.w. laser are first aligned through a 900 nm short-pass dichroic mirror and then directed into a three-dimensional laser scanner. The focused laser beams are controlled by laser scanning software to draw three-dimensional images in a transparent monolith containing the multilayer upconversion nanocrystals (0.2 wt%). The tunable colour display is realized by modulating the on/off and pulse width of the two laser inputs. **b**, Luminescence colour images generated in the nanocrystal/PDMS composite monolith show the ability to display additive colours (left) and three-dimensional objects with wide colour gamuts (right) using the as-developed display system. **c**, Schematic representation of the computational design of a volumetric full-colour three-dimensional display (left) and the true image (right) generated through use of the multilayer upconversion nanocrystals. **d**, Volumetric three-dimensional display generated by combining three sets of conventional upconversion nanoparticles featuring monochromatic RGB emission (R, $\text{KMnF}_3\text{:Yb/Er}$; G, $\text{NaYF}_4\text{:Yb/Er}$; B, $\text{NaYF}_4\text{:Yb/Tm}$). Note that mixing upconversion nanocrystals with different emission colours in a cyclohexane solution (top) or a PDMS composite monolith (bottom) only results in a white colour. Scale bars, 1 cm.

namely $^5\text{I}_6 \rightarrow ^5\text{I}_7$ relaxation, is needed to populate the $^5\text{I}_7$ state of Ho^{3+} . By comparison, the green emission from the $^5\text{F}_4, ^5\text{S}_2$ states of Ho^{3+} is likely to be populated at a much faster rate due to direct two-step energy transfer from Yb^{3+} . The difference in pumping rate between two different emitting states implies that the red/green emission ratio can be controlled by a pulse width modulation technique. It is conceivable that, with suitably adjusted short pulse duration, dominant green emission is achievable, as the cutoff in the excitation pulse prevents the onset of undesirable energy transfer from the $^5\text{I}_6$ to $^5\text{I}_7$ states of Ho^{3+} (Fig. 2). It should be noted that, in principle, the non-radiative relaxation from the $^5\text{I}_6$ to $^5\text{I}_7$ states of Ho^{3+} is a fairly slow process due to the presence of a relatively large energy gap ($\sim 3,400 \text{ cm}^{-1}$) in $\text{Yb}^{3+}/\text{Ho}^{3+}$ co-doped systems. To facilitate the non-radiative relaxation from the $^5\text{I}_6$ state of Ho^{3+} for enhanced red emission, we doped Ce^{3+} (8 mol%) along with the $\text{Yb}^{3+}/\text{Ho}^{3+}$ couple in the same layer. The utilization of Ce^{3+} benefits non-radiative relaxation through a phonon-assisted energy transfer process, as confirmed by low-temperature upconversion spectroscopic studies (Supplementary Fig. 7). Moreover, considering that the lifetime of

the excited states of Ho^{3+} is long ($>100 \mu\text{s}$, Supplementary Fig. 8), it is plausible to fine-tune the red/green emission ratio by controlling the time interval (frequency) of the excitation pulse within the range of the decay time of Ho^{3+} .

The non-steady-state upconversion mechanism proposed for Ho^{3+} emission upon pulsed excitation at 980 nm was validated by time-resolved photoluminescence studies. Under the action of a 10-ms-wide laser pulse (25 Hz), the rate of change in the red emission of Ho^{3+} was found to be appreciably slower than measured for its green emission (Fig. 3a). Quite surprisingly, we observed an abrupt drop in green emission intensity after 1 ms of laser excitation, indicating a rapid depletion of the excitation energy related to the $^5\text{F}_4, ^5\text{S}_2$ energy states of Ho^{3+} . The intensity of the green emission then gradually declines over time until its steady state is reached, after which time the emission intensity does not change upon further excitation. This experimental observation is consistent with our numerical simulation obtained using the rate equations derived from the proposed upconversion process (see Supplementary Information), strongly suggesting the existence of a non-steady-state energy transfer mechanism (Supplementary

Fig. 10). Note that similar optical phenomena involving lanthanide-doped nanomaterials have never previously been reported. The plot of red/green emission ratio as a function of excitation duration further reveals the optical dynamics of Ho^{3+} (Fig. 3b). There is a substantial optical change in the red/green emission ratio when the pulse width of the excitation reaches 450 μs . The ratio of red/green emission rises sharply and reaches the maximum level of production after 5 ms of excitation.

Power dependence investigations of the multilayer nanocrystals indicate that both red and green emissions of Ho^{3+} are governed by two-photon excitation upconversion processes (Fig. 3c). Interestingly, we found that the ratio of red/green emission is independent of excitation power density. Under excitation at 980 nm with either a c.w. or pulsed (200 μs) light source (with a peak power density in the 10–100 W cm^{-2} range), the nanocrystals did not exhibit noticeable changes in emission colour (Fig. 3d). Taken together, these results explicitly imply the possibility of accessing the colour emission of the nanocrystals with an arbitrary number of grey levels by simply adjusting the excitation power, further attesting to their versatility in colour display.

The ability of our multilayer nanocrystals to emit variable emission on demand in response to excitation wavelength and pulse width provides a convenient way of implementing the multi-primary spatial and temporal colour synthesis required for full-colour volumetric three-dimensional displays. As a proof of concept, we incorporated the nanocrystals into a polydimethylsiloxane (PDMS) monolith to construct a transparent display matrix. Due to the nonlinear nature of signal generation in photon upconversion, only nanocrystals within the focal volume of the laser beam can be excited. By supplementing the 808 nm c.w. light source with a pulse-modulated 980 nm beam, we can generate three-dimensional imagery by moving the focal point of the beam within the volume of the display matrix (Fig. 4a, Supplementary Fig. 11). Using this approach, we have been able to generate true multi-perspective colour images with high spatial resolution and precision (Fig. 4b,c). This display design is extremely convenient when compared to existing solid-state three-dimensional full-colour display techniques, which usually require stacked layers that are individually sensitive to the primary colours⁴. Additionally, the viewing capability offered by our system is not possible with holographic or glasses-based stereoscopic displays²⁸. It is worth noting that homogeneous mixing of equal amounts of nanophosphors with balanced monochromatic RGB elements in solutions or solid-state substrates only produces superimposed white colour images (Fig. 4d, Supplementary Fig. 13).

Conventional photon upconversion by lanthanide-doped materials under c.w. excitation is typically dominated by steady-state processes in which the deactivation and population of the excited states exist in equilibrium. The experimental results reported here provide clear evidence for the importance of non-steady states in controlling the excitation dynamics and ultimately luminescence emission of upconversion nanocrystals. The multilayer core-shell design, by minimizing cross-relaxation and regulating energy migration pathways, enables us to realize tunable emission with arbitrary colours and the construction of full-colour volumetric three-dimensional display from nanocrystals of fixed composition. We believe that our demonstration will provide a major step towards the precise control of colour emission and will offer tantalizing opportunities for applications in the fields of optical memory, multiplexed optical chemical sensing, security printing and potentially many others^{29–32}.

Methods

Preparation of colour-tunable core-shell upconversion nanocrystals. NaYF_4 -based core-shell nanocrystals were synthesized by a modified solvent-thermal method, and the nanocrystal/PDMS composite monoliths were prepared by a modified literature method according to ref. 33. Further experimental details are provided in Supplementary Materials and Methods.

Operating procedure for volumetric three-dimensional display. In a typical experiment, two excitation diode lasers with wavelengths of 980 and 808 nm were aligned and directed into a fast scanning three-dimensional galvanometer and refocused onto the nanocrystal/PDMS composite monolith. A digital-pulse generator was used to modulate the 980 nm laser to generate pulse-width-controllable beams with a fixed frequency of 100 Hz and variable pulse durations from 200 μs to 6 ms. During the process of volumetric three-dimensional rendering, the focused laser beam was controlled and scanned across the sample. The size of the scanning laser focal spot was determined by

$$\text{Spot Size} = 1.83 \times \lambda \times \frac{f}{A}$$

where λ is the wavelength of the laser, f is the effective focal length of the lens, and A is the entrance beam diameter. The spot resolution of this system was estimated to be $100 \mu\text{m} \times 100 \mu\text{m} \times 200 \mu\text{m}$ ($x \times y \times z$). It should be noted that the resolution can be further enhanced by optimizing the alignment of the two laser inputs to decrease the focal volume of the scanning laser spot. Scanning in the x - y plane was realized by rotating the galvanometer mirror combined with a F - θ lens (focal length = 198 mm), while z -direction scanning was achieved by modulating the dynamic beam expander (± 7 mm). The scanning pathway of the laser beam across the sample was precisely controlled by Cyberlease scanning software (IDI Laser). The colour display was tuned by controlling the pulse width of the 980 nm diode laser or switching the 808 nm c.w. diode laser on and off. The output laser power was adjusted in the range from 1 to 3 W and the scanning speed was set in the range of 1.5–6 mm s^{-1} depending on the specific images generated.

Received 29 October 2014; accepted 3 December 2014;
published online 19 January 2015

References

- Matsubara, H. *et al.* GaN photonic-crystal surface-emitting laser at blue-violet wavelengths. *Science* **319**, 445–447 (2008).
- Lee, J. *et al.* Universal process-inert encoding architecture for polymer microparticles. *Nature Mater.* **13**, 524–529 (2014).
- Park, S. *et al.* Printed assemblies of inorganic light-emitting diodes for deformable and semitransparent displays. *Science* **325**, 977–981 (2009).
- Downing, E., Hesselink, L., Ralston, J. & Macfarlane, R. A three-color, solid-state, three-dimensional display. *Science* **273**, 1185–1189 (1996).
- Kim, T. H. *et al.* Full-color quantum dot displays fabricated by transfer printing. *Nature Photon.* **5**, 176–182 (2011).
- Sun, Y. *et al.* Quantum-sized carbon dots for bright and colorful photoluminescence. *J. Am. Chem. Soc.* **128**, 7756–7757 (2006).
- Chen, O. *et al.* Excitation-intensity-dependent color-tunable dual emissions from manganese-doped CdS/ZnS core/shell nanocrystals. *Angew. Chem. Int. Ed.* **49**, 10132–10135 (2010).
- Han, S., Deng, R., Xie, X. & Liu, X. Enhancing luminescence in lanthanide-doped upconversion nanoparticles. *Angew. Chem. Int. Ed.* **53**, 11702–11715 (2014).
- Gai, S., Li, C., Yang, P. & Lin, J. Recent progress in rare earth micro/nanocrystals: soft chemical synthesis, luminescent properties, and biomedical applications. *Chem. Rev.* **114**, 2343–2389 (2014).
- Bünzli, J. C. G. & Piguet, C. Taking advantage of luminescent lanthanide ions. *Chem. Soc. Rev.* **34**, 1048–1077 (2005).
- Rapaport, A., Milliez, J., Bass, M., Cassanho, A. & Jensen, H. Review of the properties of up-conversion phosphors for new emissive displays. *J. Display Technol.* **2**, 68–78 (2006).
- Wen, H. *et al.* Upconverting near-infrared light through energy management in core-shell nanoparticles. *Angew. Chem. Int. Ed.* **52**, 13419–13423 (2013).
- Heer, S., Kömpe, K., Güdel, H. U. & Haase, M. Highly efficient multicolour upconversion emission in transparent colloids of lanthanide-doped NaYF_4 nanocrystals. *Adv. Mater.* **16**, 2102–2105 (2004).
- Li, X., Wang, R., Zhang, F. & Zhao, D. Engineering homogeneous doping in single nanoparticle to enhance upconversion efficiency. *Nano Lett.* **14**, 3634–3639 (2014).
- Wang, F. & Liu, X. Multicolor tuning of lanthanide-doped nanoparticles by single wavelength excitation. *Acc. Chem. Res.* **47**, 1378–1385 (2014).
- Haase, M. & Schäfer, H. Upconverting nanoparticles. *Angew. Chem. Int. Ed.* **50**, 5808–5829 (2011).
- Van der Ende, B. M., Aarts, L. & Meijerink, A. Lanthanide ions as spectral converters for solar cells. *Phys. Chem. Chem. Phys.* **11**, 11081–11095 (2009).
- Gargas, D. J. *et al.* Engineering bright sub-10-nm upconverting nanocrystals for single-molecule imaging. *Nature Nanotech.* **9**, 300–305 (2014).
- Ju, Q. *et al.* Amine-functionalized lanthanide-doped KGdF_4 nanocrystals as potential optical/magnetic multimodal bioprobes. *J. Am. Chem. Soc.* **134**, 1323–1330 (2012).
- Zhou, J. *et al.* Ultrasensitive polarized up-conversion of Tm^{3+} - Yb^{3+} doped β - NaYF_4 single nanorod. *Nano Lett.* **13**, 2241–2246 (2013).

21. Mahalingam, V. *et al.* Bright white upconversion emission from $\text{Tm}^{3+}/\text{Yb}^{3+}/\text{Er}^{3+}$ doped $\text{Lu}_3\text{Ga}_5\text{O}_{12}$ nanocrystals. *J. Phys. Chem. C* **112**, 17745–17749 (2008).
22. Vetrone, F., Boyer, J. C., Capobianco, J. A., Speghini, A. & Bettinelli, M. Significance of Yb^{3+} concentration on the upconversion mechanisms in codoped $\text{Y}_2\text{O}_3:\text{Er}^{3+}, \text{Yb}^{3+}$ nanocrystals. *J. Appl. Phys.* **96**, 661–667 (2004).
23. Sharma, G. & Trussell, H. J. Digital color imaging. *IEEE Trans. Image Process.* **6**, 901–932 (1997).
24. Shen, J. *et al.* Engineering the upconversion nanoparticle excitation wavelength: cascade sensitization of tri-doped upconversion colloidal nanoparticles at 800 nm. *Adv. Opt. Mater.* **1**, 644–650 (2013).
25. Wang, Y. *et al.* Nd^{3+} -sensitized upconversion nanophosphors: efficient *in vivo* bioimaging probes with minimized heating effect. *ACS Nano* **7**, 7200–7206 (2013).
26. Auzel, F. Upconversion and anti-Stokes processes with *f* and *d* ions in solids. *Chem. Rev.* **104**, 139–174 (2004).
27. Sivakumar, S., van Veggel, F. C. J. M. & May, P. S. Near-infrared (NIR) to red and green up-conversion emission from silica sol-gel thin films made with $\text{La}_{0.45}\text{Yb}_{0.50}\text{Er}_{0.05}\text{F}_3$ nanoparticles, hetero-looping-enhanced energy transfer (hetero-LEET): a new up-conversion process. *J. Am. Chem. Soc.* **129**, 620–625 (2007).
28. Fattal, D. *et al.* A multi-directional backlight for a wide-angle, glasses-free three-dimensional display. *Nature* **495**, 348–351 (2013).
29. Zhou, J., Liu, Z. & Li, F. Upconversion nanophosphors for small-animal imaging. *Chem. Soc. Rev.* **41**, 1323–1349 (2012).
30. Lu, Y. *et al.* Tunable lifetime multiplexing using luminescent nanocrystals. *Nature Photon.* **8**, 32–36 (2014).
31. Wang, J. *et al.* Near-infrared-light-mediated imaging of latent fingerprints based on molecular recognition. *Angew. Chem. Int. Ed.* **53**, 1616–1620 (2014).
32. Debasu, M. L. *et al.* All-in-one optical heater-thermometer nanoplatform operative from 300 to 2000 K based on Er^{3+} emission and blackbody radiation. *Adv. Mater.* **25**, 4868–4874 (2013).
33. Wang, F. *et al.* Simultaneous phase and size control of upconversion nanocrystals through lanthanide doping. *Nature* **463**, 1061–1065 (2010).

Acknowledgements

The work was supported by the Singapore Ministry of Education (grant no. MOE2010-T2-1-083), the Agency for Science, Technology and Research (A*STAR; grant no. 1231AFG028), the National Research Foundation and the Priority Academic Program Development of Jiangsu Higher Education Institutions, Fundamental Studies of Perovskite Solar Cells (2015CB932200), and the National Natural Science Foundation of China (grant nos. 51173081, 61136003). M.H. acknowledges the National Research Foundation, Prime Minister's Office, Singapore, for financial support under the Competitive Research Program (CRP award no. NRF-CRP10-2012-04).

Author contributions

R.D. and X.L. conceived the projects with contributions from W.H. and M.H. R.D. and F.Q. were primarily responsible for the experiments. R.C. contributed to numerical simulations. M.H. and W.H. provided input into the design of the experiments. R.D. and X.L. wrote the paper. All authors discussed the results and commented on the manuscript.

Additional information

Supplementary information is available in the [online version](#) of the paper. Reprints and permissions information is available online at www.nature.com/reprints. Correspondence and requests for materials should be addressed to W.H., M.H. and X.L.

Competing financial interests

The authors declare no competing financial interests.